Elastic Deformation in Ceria Nanorods *via* a Fluorite-to-Rutile Phase Transition

Thi X. T. Sayle and Dean C. Sayle*

DASSR, Cranfield University, Defence Academy of the United Kingdom, Shrivenham, SN6 8LA, United Kingdom

ARTICLE

ABSTRACT Atomistic simulations reveal that ceria nanorods, under uniaxial tension, can accommodate over 6% elastic deformation. Moreover, a reversible fluorite-to-rutile phase change occurs above 6% strain for a ceria nanorod that extends along [110]. We also observe that during unloading the stress increases with decreasing strain as the rutile reverts back to fluorite. Ceria nanorods may find possible application as vehicles for elastic energy storage.

KEYWORDS: atomistic simulation · microstructure · molecular dynamics · nanoenergy storage

Much effort has been applied to the study of one-dimensional nanomaterials, such as nanorods and nanotubes, because of their unique electrical,[1] chemical,[2,3] and mechanical[4] properties, compared to the parent bulk material, with applications spanning catalysis to energy storage. However, central to their application in a diverse range of applications is their mechanical durability and "perceived" fragility. Such vulnerability may reflect a structural response to, for example, friction and wear, localized compressive or tensile strain attributed to heating/cooling, operational vibration, and for intercalation hosts used to store charge carriers such as Li ions in rechargeable batteries, structural collapse under charge/discharge cycles.[5] High mechanical strength, toughness, and fracture resistance are central to the exploitation of nanomaterials in a range of applications spanning biomedical and dental[6] to MEMS.[7] Accordingly, to help meet such demanding requirements, a fundamental (atomistic) understanding of the mechanical properties and processes of nanomaterials, such as strength and fracture mechanics is needed. However, direct measurement of mechanical load is difficult experimentally—requiring *in situ* mechanical deformation testing.[8] Notwithstanding such challenges, Shokuhfar and co-workers measured the mechanical compressive properties of individual thin-wall and thick-wall TiO_2 nanotubes directly[9] and found that the Young's modulus of titanium dioxide nanotubes depended upon the diameter and wall thickness of the nanotube and is in the range of 23−44 GPa; the thin-wall nanotubes collapsed at 1.0−1.2 N during axial compression.

Atomistic computer simulation can be used to simulate mechanical deformation and is well-placed to complement experiment because the simulations are comparatively easier—molecular graphics can be used to explore the structural transformation during loading. For example, Xiong and co-workers explored uniaxial tension on MgO nanorods using molecular dynamics simulation, which revealed the atomic-scale mechanism of the deformation and failure process during tension.[10] In particular, they observed increased ductility at reduced strain rates. However, the difficulty associated with simulation is the generation of a structural model that is sufficiently realistic in that the results generated using the model are of value to experiment. Specifically, real nanorods are unlikely to be structurally perfect; rather they will contain microstructural features, such as morphology and surfaces exposed, grain-boundaries, dislocations, and point defects. Indeed, Koh and Lee predicted that the tensile strength of platinum nanowires can change by up to 50% by altering the cross-sectional shape of the nanowire.[11] Moreover, it is well-known that the (measured) strength of a material is about 2 orders of magnitude less

*Address correspondence to d.c.sayle@cranfield.ac.uk.

Received for review November 12, 2009 and accepted January 26, 2010.

Published online February 8, 2010.
10.1021/nn901612s

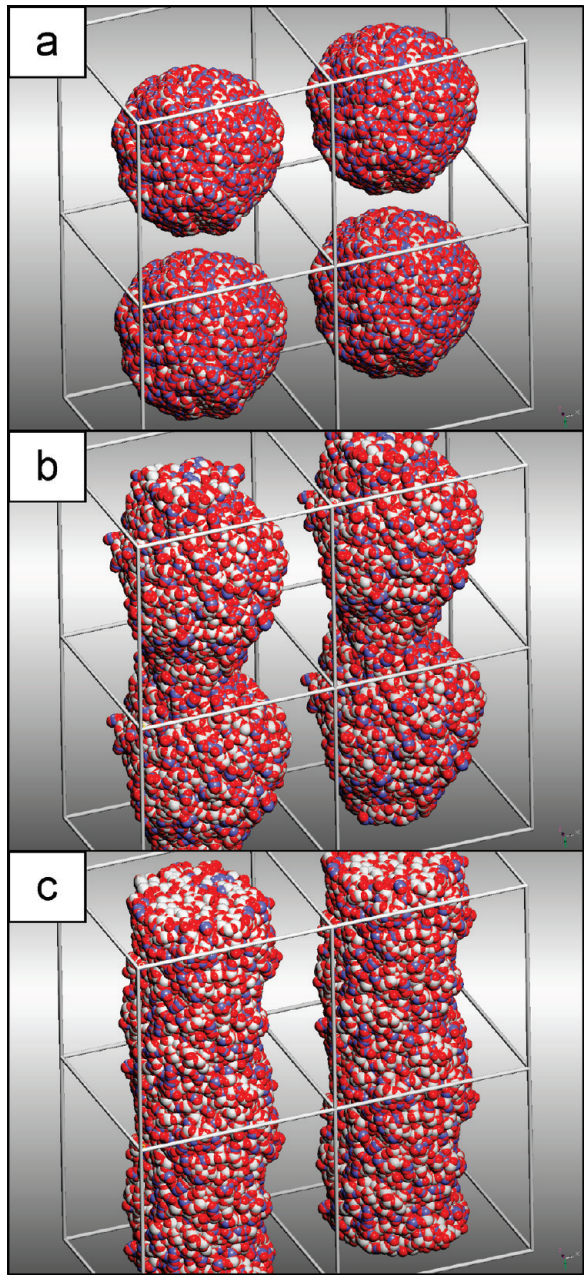

Figure 1. Strategy used to generate atomistic models for nanorods. (a) Amorphous nanoparticles positioned into simulation cell; (b) agglomeration of neighboring nanoparticles in one dimension; (c) evolution of nanorod topography; the nanorod is then crystallized. Atom positions are represented by white and blue spheres (cerium) and red spheres (oxygen). The blue spheres are used to show the high mobility of the ions within the amorphous phase.

than its estimated ideal strength. This is attributed to the presence of microstructural features, specifically dislocations, which provide vehicles for plastic deformation. On the other hand, nanomaterials can sustain stresses more than a tenth of their ideal strengths[12] because they are less able to retain a dislocation population within their (size-constrained) structure compared to their bulk counterpart.[13]

To better understand the unique mechanical properties of nanomaterials, we simulated ceria nanorods under mechanical load. Clearly, if we are to use the models to simulate and predict the mechanical properties, similar to real nanorods, the model nanorods must comprise a rich microstructure. Accordingly, to generate such models we used simulated amorphization and crystallization,[14] Figure 1, which is a simulation strategy capable of introducing a variety of microstructural features into an atomistic model, including, for example, surfaces and morphology, point defects and clusters, dislocations, and grain-boundaries. Ceria is a prototypical, chemically reactive ceramic oxide, which has been exploited extensively in a wide range of applications including fuel cells,[15] catalysts,[16] nanoabrasives,[17] and sensor.[18]

RESULTS

The structure of the crystalline CeO_2 nanorod with a [110] primary axis is shown in Figure 2a−e. The rod is about 10 nm in diameter, exposes {111} and {100} surfaces facilitating a hexagonal cross-section and extends along [110] in accord with experiment.[19] Experimentally, nanorods with [211] as the principal axis have also been synthesized.[20] We found that by crystallizing the nanorod at 3400 K instead of 3750 K yielded a model of a nanorod that extended along [211], which is shown in Figure 2f and compared to experiment in Figure 2g. This nanorod also exposes {111} and {100}.

Close inspection of the atomistic structure of the nanorods using molecular graphics, Figures 2(a, f), revealed a complex array of steps, edges and corners on the surface together with point defects that evolved both on the surface and in the bulk regions of the nanorod including cerium and oxygen vacancies and vacancy clusters. It is therefore evident that the simulated crystallization procedure has enabled microstructural features to be captured within the model nanorods and therefore we expect these models to display behavior, which is more realistic compared to the real material.

Tensile Loading. The behavior of the nanorods under mechanical load is shown in Figure 3. The blue (loading) trace and green (unloading) trace correspond to the nanorod with a principal axis along [110], Figure 2a, whereas the red (loading) trace corresponds to the nanorod with a principal axis along [211], Figure 2f.

CeO_2 Nanorod with [110] Principal Axis. Inspection of the stress−strain curves reveal a yield strain of 0.066 with an associated tensile strength of about 18 GPa. The stress−strain trace is curved, which reflects a reduced Youngs modulus with increased strain. Inspection of the nanorod during tensile strain reveals that "crack" formation emanates from the surface (Figure 4a). However, surprisingly, upon increased strain, the CeO_2 at the crack region undergoes a polymorphic transformation from fluorite to rutile (Figure 4b). Moreover rather

than suffering complete fracture, the nanorod maintains mechanical strength for a further 0.03 strain, at which point the simulation was stopped. Similar to a "concertina", the nanorod accommodates the strain *via* this phase change (images showing more clearly the fluorite and rutile-structured CeO_2 are shown in Figure 4c; a view looking perpendicular to the structure in 4c is shown in 4d).

In Figure 5, a region near the "crack" is enlarged to reveal more clearly the mechanism underpinning the fluorite−rutile phase transformation. In particular, Figure 5a shows the atomistic structure of a region of the CeO_2 nanorod (3200 ps, strain = 0.064) that conforms to the fluorite structure, which transforms to rutile after a further 12.5 ps, Figure 5b. Side views of Figure 5 panels a and b are shown in panels c and d, respectively.

We note that the molecular graphics shown in this study are not schematics; rather they are representations of the atom positions. In addition, to improve the clarity of the images, segments were cut from the full system because (for example) surface relaxation and subtle curvatures of the atoms comprising the nanorod can obscure the polymorphic crystal structures. Time averaged thermal ellipsoids can be generated using the raw data. However, they also obscure structural clarity; rather the images presented are "snapshots" captured at a particular instants in time.

CeO_2 Nanorod with [211] Principal Axis. The stress−strain curve for these nanorods, Figure 3, reveals a yield strain of about 0.062 with an associated tensile strength of 21 GPa. A fluorite-to-rutile phase change was not observed for this nanorod. Moreover, the trace at the yield point is sharper compared to the nanorods with the [110] primary axis.

Unloading. The unloading trace, which was performed at the same strain rate (10^7 s^{-1}) as tensile loading, is shown in green on Figure 3 for the CeO_2 nanorod with a principal axis along [110]. The figure shows that the strain of 0.09 is not wholly elastic, rather the nanorod remains strained by about 0.04, compared to the starting structure, at zero stress. Analysis of the unloading, using graphical techniques, reveals that the domain corresponding to the rutile polymorph reverts back to fluorite between about 0.07 and 0.055 strain (Figure 6 and Figure 7). Surprisingly, the stress−strain trace corresponding to this reverse phase transition (Figure 3) shows an *increase* in stress as the strain is reduced. This may be explained when one considers that cerium is coordinated to eight oxygen in fluorite, whereas in rutile, cerium is only six coordinate.

Further simulations, where the nanorod was tensioned uniaxially above a strain of 0.09, revealed that the rutile polymorph transformed structurally back to the fluorite structure; the structure of the nanorod after 0.12 strain is shown in Figure 8. Animations of the ceria nanorod under tensile strain, showing more clearly the mechanism underpinning the fluorite-to-rutile phase transformation, are available in Supporting Information.

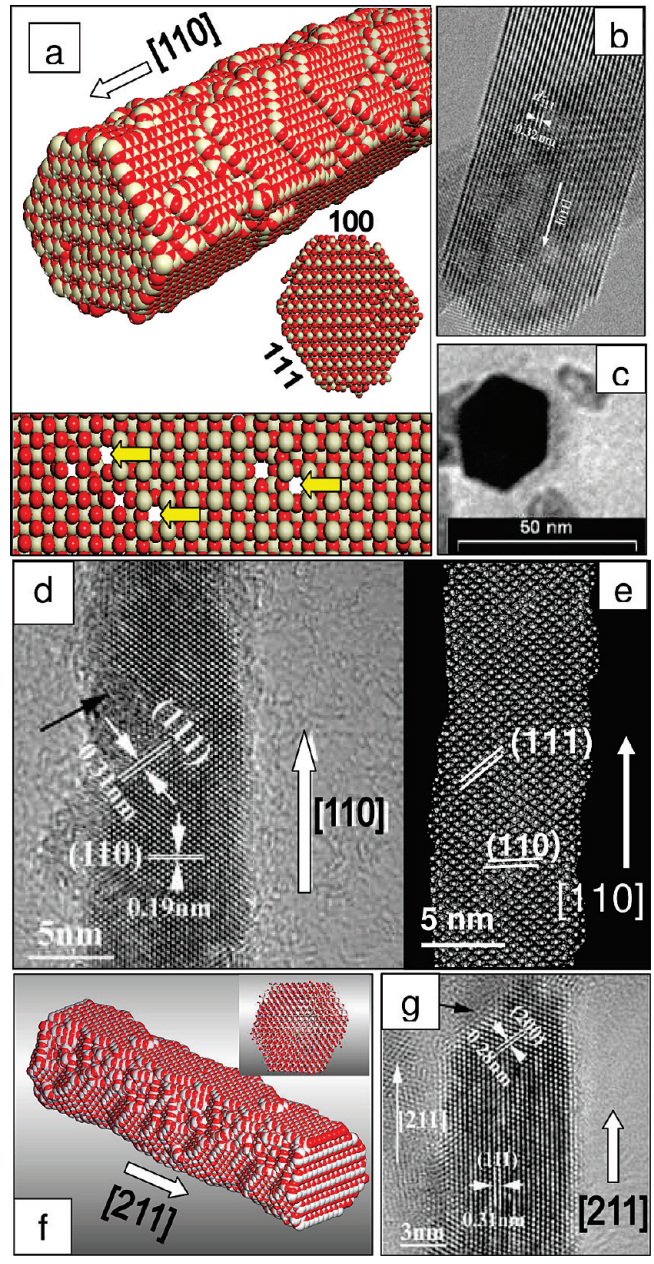

Figure 2. Models of the ceria nanorods compared with experiment. (a) Atomistic model of the nanorod that extends along [110]: (top) perspective view; (middle) view looking along [110] revealing the hexagonal profile of the nanorod; (bottom) slice cut through the nanorod revealing the Ce and O vacancies that have evolved in the nanorod during (simulated) crystallization. (b, c) HRTEM images taken from ref 19; (d) HRTEM showing the [110] direction taken from ref 20; (e) atomistic model to compare with panel d. In panel a, the atom positions are represented by white spheres (cerium) and red spheres (oxygen). In panel e, only the cerium atoms are shown. Panel f shows the atomistic model of the CeO_2 nanorod, which extends along [211], compared to experiment (g) taken from ref 20.

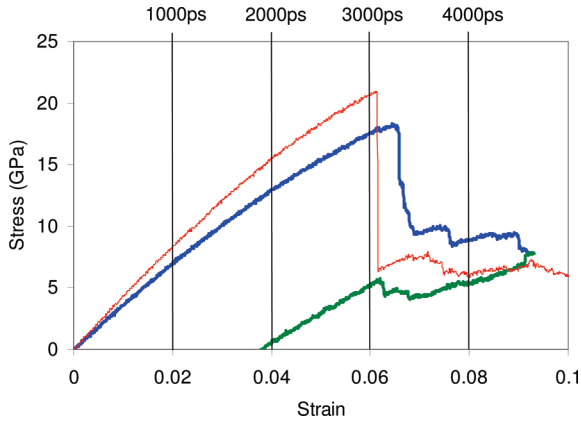

Figure 3. Stress–strain curve, calculated for a ceria nanorod under tension; the secondary (top) *x*-axis shows simulation time. The blue (tensile loading) and green (unloading) trace correspond to the CeO_2 nanorod with [110] as the primary axis; the red trace corresponds to loading of the CeO_2 nanorod with [211] as its primary axis.

DISCUSSION

Changes in atomistic structure have been reported for nanorods under strain. In particular, in a gold nanowire, simulated under tension, a ccp to b.c.t.1 packing of the metal atoms was predicted;[21] amorphization of SiC nanowires was observed under deformation;[22] rutile-to-fluorite structural transformations in SnO_2 nanorods and nanobelts under 35 GPa compression have also been observed.[23] Crucially, the authors observed that the behavior of the nanomaterial was (sometimes profoundly) different compared to the parent (bulk) material. Moreover, Agrawal and co-workers reported a wurtzite to body-centered tetragonal phase change in ZnO nanowires.[24] We therefore propose that a fluorite-to-rutile phase transformation in CeO_2 nanorods under tension is not unreasonable. In particular, rutile is less dense than fluorite and therefore this phase change offers a mechanism for relieving the strain on the nanorod; we await experimental confirmation.

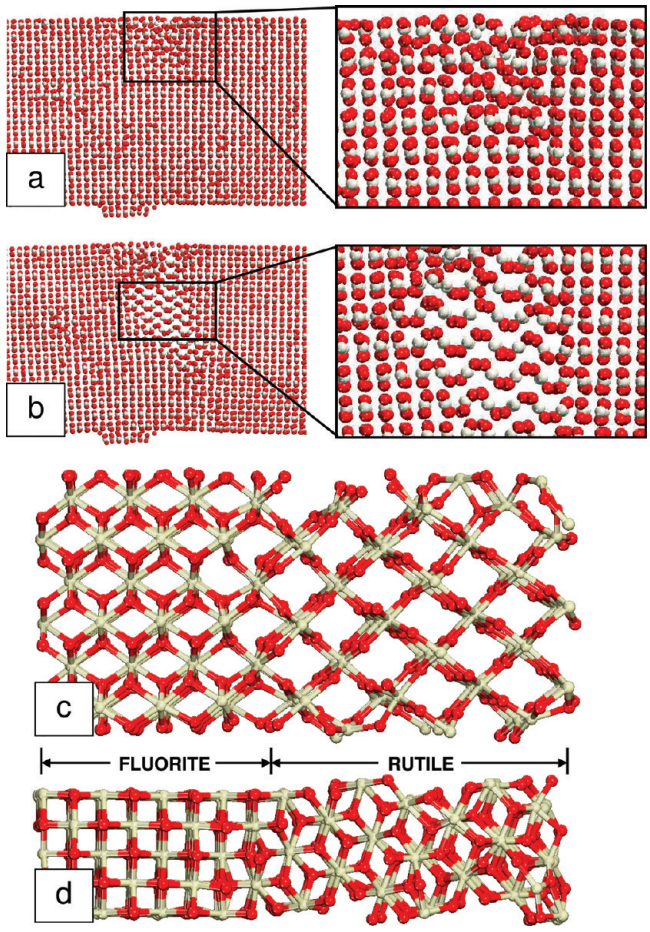

Figure 4. Atomistic structure of the ceria nanorod, with [110] as its primary axis, under tension: (a) after 3187 ps (strain 0.0637); (b, c, d) after 3212.5 ps (strain 0.0643); panels c and d show an enlarged segment of panel b. The structures can be usefully correlated with the stress–strain trace shown in Figure 3. Cerium is colored white and oxygen is red; (a,b) sphere model representations of the atom positions; (c,d) ball and stick model representations.

We note that the strain rate associated with our simulations is high, which will likely influence the mechanical behavior of the nanorods and may explain the surprisingly high elasticity of ceria nanorods. Conversely, while ceramic materials are brittle at room temperature and usually fracture at strains of less than 0.1%, at the nanoscale the mechanical properties can change profoundly. In particular, Han and co-workers observed large strain plasticity in ceramic SiC nanowires.[22] The mechanism of the plasticity was observed to be associated with the evolution of dislocations. In addition, MgO nanorods were predicted to be more brittle at higher strain rate.[10] A study by Wolf and co-workers reviews mechanical deformation, simulated using MD, compared with experiment.[25]

That the [211] did not undergo a fluorite to rutile phase change raises an interesting question as to what role each structural feature (morphology, point defect, or rod "growth" direction) has with respect to the phase change; the morphology of the ceria nanorods with a primary axis along [211] differs compared to the nanorods with primary axis along [110] (Figure 2a,f), slight changes in the (point) defect distribution also exists between the two models. To help answer this question, an exhaustive screening of structure against phase change would need to be performed. Normally, atomistic computer simulation is a technique that is well suited to test many (sometimes thousands using grid computing) different configurations. However, here the generation of the model, using simulated crystallization, is difficult and time-consuming, and its development has not yet matured to a point of automation. Moreover, each deformation simulation required about 6000cpu hours. Accordingly, such a study must await the maturation of the technique and an increase in computational performance.

The validity of to the fluorite-to-rutile phase change, predicted in this study, rests critically upon

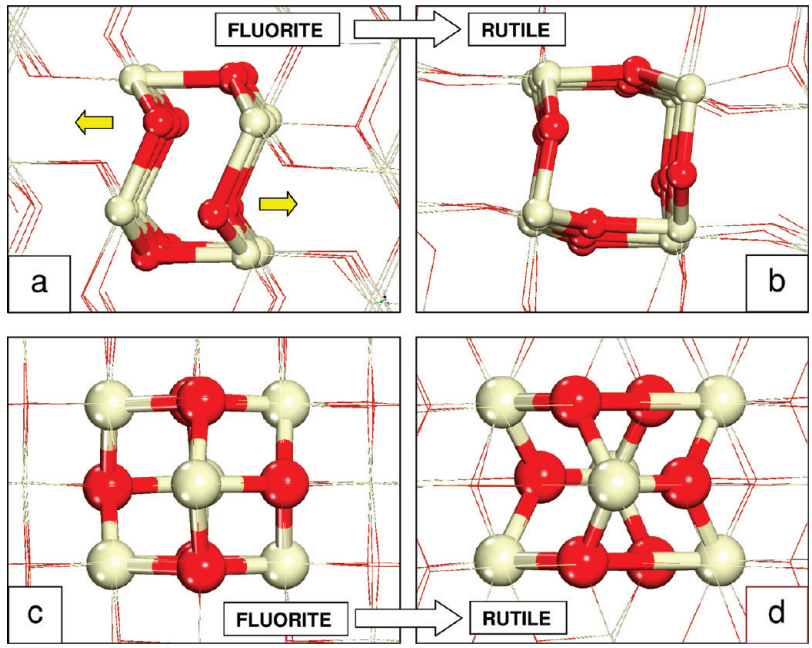

Figure 5. Atomistic structure of the ceria nanorod showing more clearly the fluorite−rutile phase transformation: (a) fluorite structure (3200 ps, 0.064 strain), (b) rutile structure (3212.5 ps, 0.0643 strain), (c) side view of panel a, (d) side view of panel b.

the interatomic potentials used to model the ceria nanorod. Accordingly, simulating the system using a quantum mechanical description, such as density functional theory (DFT), will provide further support to the possibility that real nanorods oriented along [110] will undergo such a phase change under uniaxial tension. However, we have shown that such behavior is influenced by the atomistic structure, microstructure, and morphology of the nanorod. Specifically, nanorods oriented along [211] did not undergo a fluorite−rutile phase change. Accordingly, if one were to mirror the simulations per-

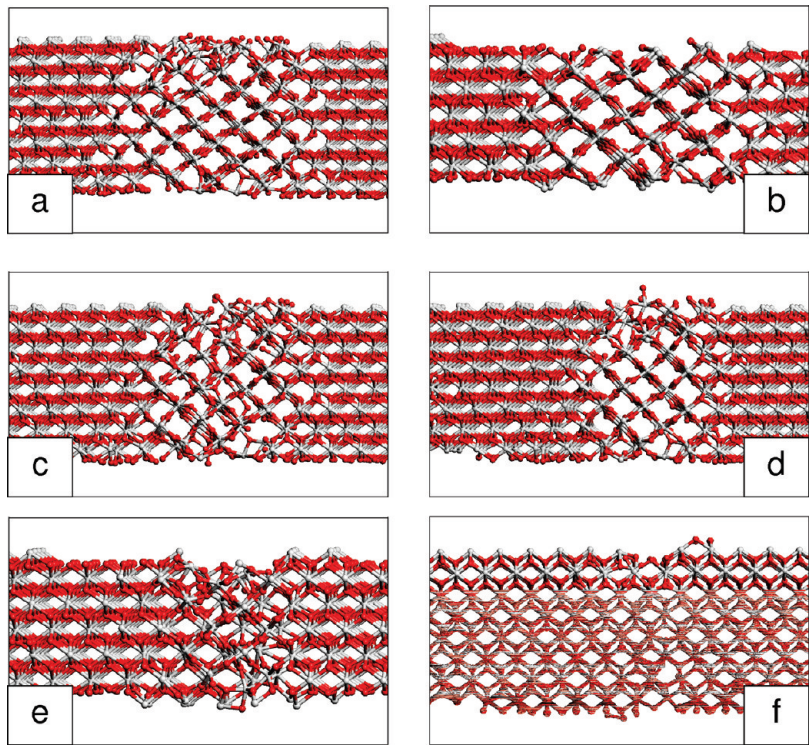

Figure 6. Ball and stick representations of the atom positions comprising a segment of the ceria nanorod, with a primary axis along [110], during unloading. Snapshots taken at a strain of (a) 0.093, (b) 0.083, (c) 0.068, (d) 0.063, (e) 0.058, and (f) 0.038. The images can be usefully correlated to the green unloading trace in Figure 3.

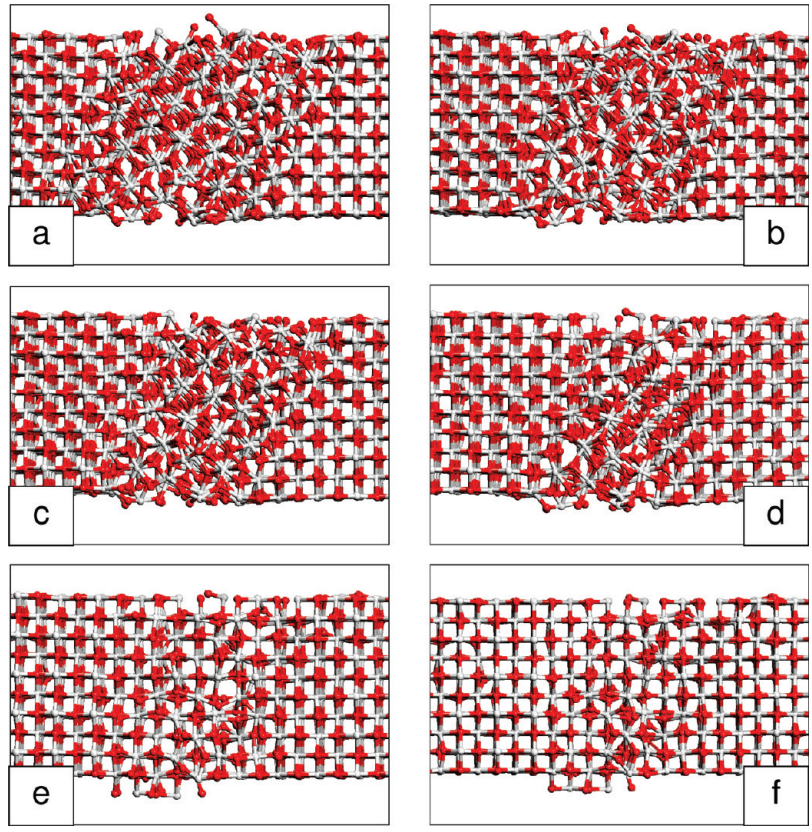

Figure 7. Ball and stick representations of the atom positions comprising a segment of the ceria nanorod, with a primary axis along [110], during unloading (side view of Figure 6). Snapshots taken at a strain of (a) 0.093, (b) 0.068, (c) 0.063, (d) 0.058, (e) 0.053, and (f) 0.038. The images can be usefully correlated to the green unloading trace in Figure 3.

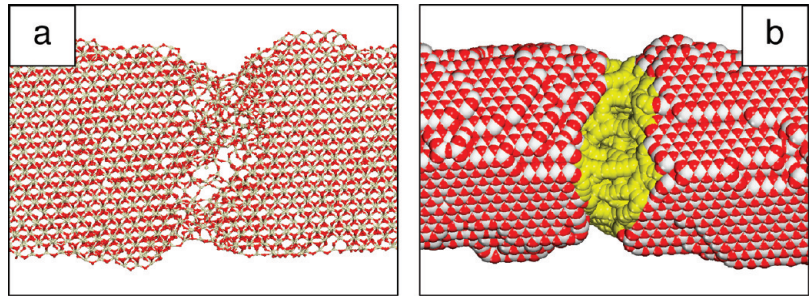

Figure 8. Structure of the ceria nanorod, with [110] as the primary axis, after 0.12 strain. (a) Slice cut through the nanorod revealing more clearly the crystal structure; (b) sphere model representation of the nanorod. We note that the rutile polymorph is no longer evident; rather the nanorod conforms to a fluorite structure. Cerium is colored white and oxygen is red. The yellow highlights the deformed region.

formed here using, for example, DFT, then the model would need to include the structural complexity of the atomistic models used in this present study.

The elasticity of the ceria nanorods may find possible application as vehicles for nanoenergy storage.[26] In particular, Hill and co-workers evaluated "forests" of carbon nanotubes and predicted that they can be used to store elastic energy 3 orders of magnitude greater than the maximum energy density of steel springs and eight times greater than the energy density of lithium-ion batteries. Applications may include supplying mechanical energy in, for example, automatic mechanical watches, "flapping wing" artificial flight[27] and MEMS devices.

CONCLUSION

Most bulk ceramic materials, such as ceria (CeO_2) are brittle, which can impact severely upon their exploitation in a variety of applications. However, we predict that CeO_2 nanorods deform elastically up to 6% tensile strain. Moreover, above this level of strain, the CeO_2 nanorod, which extends along [110], undergoes a fluorite-to-rutile phase transformation.

Upon release of the stress, domains of rutile-structured CeO_2 transform back to the fluorite polymorph. Surprisingly, the simulations predict an increase in stress as the strain is relieved during unloading, which is indicative of the rutile-to-fluorite transformation.

METHODS

In this section we outline the potential model used to describe the ceria; the computer code used to perform the molecular dynamical simulations; the approach to generating a fully atomistic model of a ceria nanorod, which comprises a complex microstructure; and finally the mechanism for performing the simulated deformation under uniaxial loading and unloading.

Potential Model. All calculations, presented in this study, were based upon the Born model of the ionic solid, where the energy, E, of the system is given by

$$E(r_{ij}) = \sum_{ij} \frac{Q_i Q_j}{4\pi\varepsilon_o r_{ij}} + \sum_{ij} A \exp\left(\frac{-r_{ij}}{\rho}\right) - C r_{ij}^{-6}$$

where the first term represents the Coulombic interaction between ion i of charge Q_i and ion j of charge Q_j, which are a distance r_{ij} apart. This functional form is very slowly convergent and therefore the Ewald summation, with an accuracy of 10^{-6}, was used to increase the speed of convergence and reduce computational cost. The second term is of the Buckingham form, which is particularly effective in representing ionic solids. Model parameters,[28] used to describe CeO_2, are presented in Table 1. These parameters were fitted to experimental data, and therefore the hypersurface they describe is generally most accurate in the vicinity of the fit. Normally, as was the case for ceria, the parameters were fitted to the low-temperature (perfect) crystal structure. Accordingly, at interatomic separations away from equilibrium distances, the potential model may prove less reliable.[29] Clearly, to have confidence in the results, the potential model is required to accurately represent the ceria at interionic separations, which differ from the low-temperature equilibrium values.

A particularly exacting test of how accurately the force field maps the energy hypersurface is to simulate the crystallization of a nanoparticle starting from a molten precursor. In particular, previously we showed that a molten ceria nanoparticle crystallizes into a polyhedral nanocrystal in quantitative agreement with experiment.[17] Specifically, the simulation yielded the structure of a crystalline seed, which spontaneously evolved and nucleated the amorphous nanoparticle into a nanocrystal. Moreover, the polymorphic structure, morphology, and surfaces exposed were correctly generated, from an amorphous precursor, during the simulation. We note that during an amorphous−crystalline phase change simulation, bond distances deviated considerably (over 10%) from the perfect crystal.[30] This study showed that the potential model is capable of simulating accurately the dynamical behavior of ceria across a broad region of the potential hypersurface, including a phase transformation.

We also note that the O−O potential used in this study was not derived specifically for ceria; rather this transferable potential was derived against a range of metal oxides and has been successfully used to model a variety of oxides.[31] The ceria potential has been used extensively over the past 20 years to model nanorods[32] and nanotubes[33] and for calculating important properties including oxygen mobility[33] and defect formation energies.[28] Accordingly, we argue that the potential describes accurately the potential hypersurface for a broad range of interatomic distances and is therefore well suited to this present study proffering more confidence in the prediction of the remarkable elastic properties and phase change associated with a ceria nanorod.

TABLE 1. Interionic Potential Parameters, of the Form $E(r_{ij}) = \sum_{ij}(Q_iQ_j)/(4\pi\varepsilon_o r_{ij}) + \sum_{ij} A \exp(-r_{ij}/\rho) - C r_{ij}^{-6}$, Used To Describe the Ceria Nanorods

atom i	atom j	A (eV)	ρ (Å)	C (eV.Å^6)	cut-off (Å)
O	O	22764.30	0.149	27.89	10.0
O	Ce	1986.83	0.351	20.40	10.0
Ce	Ce	set to zero			

atom	mass (amu)	charge (e)
O	16.00	−2.0
Ce	140.12	+4.0

Simulation Code. The DL_POLY code was used to perform all the molecular dynamics (MD) simulations;[34] the user manual provides comprehensive analytical descriptions and discussion of the molecular dynamics simulations, force fields, boundary conditions, algorithms, and parallelization methods used in these simulations.

Three-dimensional periodic boundary conditions were used to represent the nanorod, which repeats infinitely along the length of the rod. Accordingly, the rod has neither a head nor tail and the simulation thus comprises a periodic array of parallel rods; the size of the periodic repeat, perpendicular to the rod, needs to be chosen carefully to balance computational cost, yet minimize artificial interactions between its periodic neighbors. Here, we chose a value of 9.6 nm; the periodic repeat along the length of the rod was also 9.6 nm.

Atomistic Model Generation. To generate a ceria nanorod, a "cube" of CeO_2, comprising 15972 atoms (5324 Ce, 10 648 O), was cut from the parent material and the system melted by applying constant volume MD simulation at high temperature (8000 K); the simulation cell size was sufficiently large to ensure the nanoparticle does not feel any (repulsive or attractive) interaction from its periodic neighbors (Figure 1a). The size of the simulation cell was then reduced in one dimension to enable the nanoparticle to interact and agglomerate with its periodic neighbors (Figure 1b).[32] MD simulation, performed on the system for 1000 ps at 8000 K, facilitated the evolution of the nanorod (Figure 1c). The nanorod was then crystallized by performing MD simulation at 3750 K to yield a nanorod with [110] as its principal axis or 3400 K, which resulted in a nanorod that extended along [211]. Simulated crystallization was performed for sufficient a duration to converge the energy. Molecular graphics was used to examine the atomistic structure, and nanorods that comprised dislocations or grain-boundaries were discarded because they are likely to weaken the nanorods because dislocations are vehicles for plastic deformation. Nanorods comprising dislocations and/or grain-boundaries will be considered in a future study. Molecular graphics were performed using VMD[35] and Materials Studio.

Deformation Simulation. The mechanical properties of the nanorod were calculated by equilibrating the system to the target temperature by performing constant pressure MD simulation at 300 K for 100 ps with 25 ps equilibration, prior to simulating tensile strain, which was achieved by sequential scaling of the atom coordinates and performing constant volume MD simulation at 300 K using a Nosé-Hoover thermostat;[36] a strain rate of about 10^7 s^{-1} was attained. Unloading of the tensile strain was performed in an analogous fashion.

Acknowledgment. This work was supported by EPSRC Grants EP/H001220, EP/H001298, and EP/H005838.

Supporting Information Available: S1: animation showing a ceria nanorod undergoing a fluorite-rutile phase transformation; S2: animation showing the fracture of a ceria nanorod. This material is available free of charge *via* the Internet at http://pubs.acs.org.

REFERENCES AND NOTES

1. Xia, Y. N.; Yang, P. D.; Sun, Y. G.; Wu, Y. Y.; Mayers, B.; Gates, B.; Yin, Y. D.; Kim, F.; Yan, Y. Q. One-Dimensional Nanostructures: Synthesis, Characterization, and Applications. *Adv. Mater.* **2003**, *15*, 353–389.
2. Zhou, K. B.; Wang, X.; Sun, X. M.; Peng, Q.; Li, Y. D. Enhanced Catalytic Activity of Ceria Nanorods from Well-Defined Reactive Crystal Planes. *J. Catal.* **2005**, *229*, 206–212.
3. Liu, X. W.; Zhou, K. B.; Wang, L.; Wang, B. Y.; Li., Y. D. Oxygen Vacancy Clusters Promoting Reducibility and Activity of Ceria Nanorods. *J. Am. Chem. Soc.* **2009**, *131*, 3140.
4. Riaz, M.; Fulati, A.; Amin, G.; Alvi, N. H.; Nur, O.; Willander, M. Buckling and Elastic Stability of Vertical ZnO Nanotubes and Nanorods. *J. Appl. Phys.* **2009**, *106*, 034309.
5. Debart, A.; Paterson, A. J.; Bao, J.; Bruce, P. G. α-MnO_2 Nanowires: A Catalyst for the O-2 Electrode in Rechargeable Lithium Batteries. *Angew. Chem., Int. Ed.* **2008**, *47*, 4521–4524.
6. Benzaid, R.; Chevalier, J.; Saddaoui, M.; Fantozzi, G.; Nawa, M.; Diaz, L. A.; Torrecillas, R. Fracture Toughness, Strength and Slow Crack Growth in a Ceria Stabilized Zirconia−Alumina Nanocomposite for Medical Applications. *Biomaterials* **2008**, *29*, 3636–3641.
7. Evans, A.; Bieberle-Hutter, A.; Rupp, J. L. M.; Gauckler, L. J. Review on Microfabricated Microsolid Oxide Fuel Cell Membranes. *J. Power Sources* **2009**, *194*, 119–129.
8. Lockwood, A. J.; Inkson, B. J. *In Situ* TEM Nanoindentation and Deformation of Si-Nanoparticle Clusters. *J. Phys. D* **2009**, *42*, 035410.
9. Shokuhfar, T; Arumugam, G. K.; Heiden, P. A.; Yassar, R. S.; Friedrich, C. Direct Compressive Measurements of Individual Titanium Dioxide Nanotubes. *ACS Nano* **2009**, *3*, 3098–3102.
10. Xiong, L. M.; Chen, Y. P.; Lee, J. D. Atomistic Measure of the Strength of MgO Nanorods. *Theor. Appl. Fract. Mech.* **2006**, *46*, 202–208.
11. Koh, S. J. A.; Lee, H. P. Effects of Cross-Sectional Shape and Temperature on Mechanical Behavior of Platinum Nanowires. *J. Comput. Theor. NanoSci.* **2008**, *5*, 1387–1397.
12. Shan, Z. W.; Adesso, G.; Cabot, A.; Sherburne, M. P.; Asif, S. A. S.; Warren, O. L.; Chrzan, D. C.; Minor, A. M.; Alivisatos, A. P. Ultrahigh Stress and Strain in Hierarchically Structured Hollow Nanoparticles. *Nat. Mater.* **2008**, *7*, 947–952.
13. Suresh, S.; Li, J. Material Science Deformation of the Ultrastrong. *Nature* **2008**, *456*, 716–717.
14. Sayle, T. X. T.; Catlow, C. R. A.; Maphanga, R. R.; Ngoepe, P. E.; Sayle, D. C. Generating MnO_2 Nanoparticles Using Simulated Amorphization and Recrystallization. *J. Am. Chem. Soc.* **2005**, *127*, 12828–12837.
15. Evans, A.; Bieberle-Huetter, A.; Rupp, J. L. M.; Gauckler, L. J. Review on Microfabricated Micro-Solid Oxide Fuel Cell Membranes. *J. Power Sources* **2009**, *194*, 119–129.
16. Esch, F.; Fabris, S.; Zhou, L.; Montini, T.; Africh, C.; Fornasiero, P.; Comelli, G.; Rosei, R. Electron Localization Determines Defect Formation on Ceria Substrates. *Science* **2005**, *309*, 752–755.
17. Feng, X. D.; Sayle, D. C.; Wang, Z. L.; Paras, M. S.; Santora, B.; Sutorik, A. C.; Sayle, T. X. T.; Yang, Y.; Ding, Y.; Wang, X. D.; Her, Y. S. Converting Ceria Polyhedral Nanoparticles into Single-Crystal Nanospheres. *Science* **2006**, *312*, 1504–1508.
18. Barreca, D.; Gasparotto, A.; Maccato, C.; Maragno, C.; Tondello, E.; Comini, E.; Sberveglieri, G. Columnar CeO_2 Nanostructures for Sensor Application. *Nanotechnology* **2007**, *18*, 125502.
19. Vantomme, A.; Yuan, Z. Y.; Du, G. H.; Su, B. L. Surfactant-Assisted Large-Scale Preparation of Crystalline CeO_2 Nanorods. *Langmuir* **2005**, *21*, 1132–1135.
20. Du, N.; Zhang, H.; Chen, B. G.; Ma, X. Y.; Yang, D. R. Ligand-Free Self-Assembly of Ceria Nanocrystals into Nanorods by Oriented Attachment at Low Temperature. *J. Phys. Chem. C* **2007**, *111*, 12677–12680.
21. Diao, J. K.; Gall, K.; Dunn, M. L. Surface-Stress-Induced Phase Transformation in Metal Nanowires. *Nat. Mater.* **2003**, *2*, 656–660.
22. Han, X. D.; Zhang, Y. F.; Zheng, K.; Zhang, X. N.; Zhang, Z.; Hao, Y. J.; Guo, X. Y.; Yuan, J.; Wang, Z. L. Low-Temperature *in Situ* Large Strain Plasticity of Ceramic SiC Nanowires and Its Atomic-Scale Mechanism. *Nano Lett.* **2007**, *7*, 452–457.
23. Dong, Z. H.; Song, Y. Pressure-Induced Morphology-Dependent Phase Transformations of Nanostructured Tin Dioxide. *Chem. Phys. Lett.* **2009**, *480*, 90–95.
24. Agrawal, R.; Peng, B. and; Espinosa, H. D. Experimental-Computational Investigation of ZnO Nanowires Strength and Fracture. *Nano Lett.* **2009**, *9*, 4177–4183.
25. Wolf, D.; Yamakov, V.; Phillpot, S. R.; Mukherjee, A.; Gleiter, H. Deformation of Nanocrystalline Materials by Molecular Dynamics Simulation: Relationship to Experiments. *Acta Mater.* **2005**, *53*, 1–40.
26. Hill, F. A.; Havel, T. F.; Hart, A. J.; Livermore, C. Storing Elastic Energy in Carbon Nanotubes. *J. Micromech. Microeng.* **2009**, *19*, 094015.
27. Madangopal, R; Khan, Z. A.; Agrawal, S. K. Energetics-Based Design of Small Flapping-Wing Air Vehicles. *IEEE-ASME Trans. Mechatron.* **2006**, *11*, 433–438.
28. Sayle, T. X. T.; Parker, S. C.; Catlow, C. R. A. The Role of Oxygen Vacancies on Ceria Surfaces in the Oxidation of Carbon Monoxide. *Surf. Sci.* **1994**, *316*, 329–336.
29. Gale, J. D. Gulp. Capabilities and Prospects Z. *Kristallogr.* **2005**, *220*, 552–554.
30. Sayle, D. C.; Maicaneanu, S. A.; Watson, G. W. Atomistic Models for CeO2(111), (110), and (100) Nanoparticles, Supported on Yttrium-Stabilized Zirconia. *J. Am. Chem. Soc.* **2002**, *124*, 11429–11439.
31. Lewis, G. V. Catlow, C. R. A. Potential Models for Ionic Solids, J. Phys. C: Solid State Phys. 1985, *18*, 1149−1161.
32. Sayle, D. C.; Feng, X. D.; Ding, Y.; Wang, Z. L.; Sayle, T. X. T. Simulating Synthesis: Ceria Nanosphere Self-Assembly into Nanorods and Framework Architectures. *J. Am. Chem. Soc.* **2007**, *129*, 7924–7935.
33. Martin, P.; Parker, S. C.; Sayle, D. C.; Watson, G. W. Atomistic Modeling of Multilayered Ceria Nanotubes. *Nano Lett.* **2007**, *7*, 543–546.
34. Smith, W.; Forester, T. R. *DL_POLY*; Council for the Central Laboratory of the Research Councils, Daresbury Laboratory: Daresbury, Warrington, UK 1996; www.cse.clrc.ac.uk/msi/software/DL_POLY/.
35. Humphrey, W.; Dalke, A.; Schulten, K. VMD−Visual Molecular Dynamics. *J. Mol. Graphics* **1996**, *14*, 33–38.
36. Hoover, W. G. *Phys. Rev., A* **1985**, *31*, 1695–1697.